Fluorescence monitored voltammetry of single attolitre droplets

Christopher Batchelor-McAuley,‡ Christopher A. Little,‡ Stanislav V. Sokolov, Enno Kätelhön, Giorgia Zampardi and Richard G. Compton*

Department of Chemistry, Physical and Theoretical Chemistry Laboratory, Oxford University, South Parks Road, Oxford OX1 3QZ, U.K.

ABSTRACT: The lipid soluble fluorophore Nile Red (9-diethylamino-5-benzo[α]phenoxazinone) is used to fluorescently and electrochemically label an organic-in-water emulsion, where the organic phase is an ionic liquid [P6,6,6,14][FAP]/toluene mixture. The optical detection of the individual droplets is enabled facilitating the in-situ tracking and sizing of the suspended particles (average diameter = 530 nm, interquartile range = 180 nm). Through the use of a combined thin-layer optical/electrochemical cell, the irreversible accumulation of the droplets at an optically opaque carbon fibre electrode (diameter ~ 7.5 μm) can be monitored. Potentiostatic control of the system enables the fluorescence of the surface bound particles to be electrochemically switched via control of the redox state of the dye. Subsequent measurements of the individual particle fluorescence intensities as a function of the applied electrode potential enables construction of an effective – dynamically recorded – cyclic voltammogram of an *individual* particle. The confined volume voltammetry (ca. tens of attolitres) yields insight into the asymmetry of the kinetics of the redox switching process, where it is proposed that the reformation of the fluorescent Nile Red becomes chemically "gated" in the organic phase.

The electrochemical detection of single entities is a rapidly developing research frontier[1,2] in which, to date, a host of systems have been successfully investigated including, but not limited to: electrocatalytic molecular amplification by solid nanoparticles[3], direct stochastic nanoparticle redox measurement,[4] photochemical charge transfer from nano-semiconductors,[5] indirect particle detection through diffusional blocking of a Faradaic process,[6] detection of soft colloidal[7,8] and biological[9,10] systems and, the magnetic control[11] and accumulation[12] of nanoparticles. Concomitant with these advancements an increasing amount of work is focused upon the combination of these electrochemical single entity detection procedures with optical techniques. Notable examples include: the combined fluorescence detection of single microparticle/electrode impacts,[13] spectroelectrochemical[14] and surface plasmon microscopy[15] measurements of individual surface adhered silver nanoparticles, holographic 3D particle tracking of silver nanoparticle electrochemical dissolutions[16,17] and, the combined electrochemical and electro-chemiluminescence detection of single impacts of emulsion droplets.[18] The use of optical techniques aims to provide additional and complementary information regarding the character of the particle beyond its electrochemical identification.

Ultimately the motivation driving many of these single entity investigations is a desire for the attainment of stochastic information about a population so as to yield insight into the heterogeneity of a sample. However, the vast majority of the single entity electrochemical detection procedures are predicated upon the use of chronoamperometry so as to temporally decouple the capacitive charging of the substrate electrode from the response of the generally far smaller single entity. Upon arrival and in many cases electrical contact of the single analyte at the electrode surface, a step or spike (blip) in the current-time transient is recorded. The magnitude of this electrical signal *may*[19] yield analytically useful information regarding the properties of the nano- or micro-scale material. Although the information is recorded stochastically, the use of chronoamperometry means that the response of each particle is only measured at a single electrode potential. Hence, obtaining a measurement of the electron transfer kinetics requires multiple measurements to be performed at a series of different electrode potentials and for the *average* particle response to be calculated as a function of the applied potential.[20,21] In such a manner the electrochemical kinetic information of a single particle is unobtainable and only the ensemble response may be measured. Recent work from some of the authors has demonstrated how the electrocatalytic cyclic voltammetric response of a single palladium coated carbon nanotube can be measured so as to obtain insight into the electron transfer kinetics of the single entity.[22] This methodology may provide a route by which newly synthesized nanomaterials can be characterized in the absence of a need to rigorously account for the mass-transport related complications arising from measurements made at an ensemble or composite of nanoparticles.[23,24] However, for other systems the development of alternate routes to stochastically obtain the response of single particle as a function of the applied potential is desirable.

The electrochemistry of redox active microdroplets and emulsions has an extensive history.[25] Both Marken[26] and Scholz[27,28] have provided seminal contributions towards the measurement and understanding of the voltammetry of immobilised non-electrolyte containing oil phase microdroplets. In this experiment electron transfer occurs at the three-phase boundary between the electrode, organic and aqueous phase. The coupling

of the measurement of the electrochemistry of these picolitre and sub-picolitre sized droplets with optical techniques is best exemplified by the work of Nakatani and co-workers. [29,30] This work demonstrates how by using laser techniques single droplets may be trapped and attached to an electrode surface. Subsequent measurement of the absorption spectra allows determination of the kinetics and thermodynamics of ion transfer across the organic/aqueous phase boundary.

In many experimental cases the coupling of electrochemical and optical techniques has been found to be partially limited by the requirement of using transparent or semi-transparent electrodes, such as indium tin oxide[14,26] or thin-film gold[15,17]. In contrast, epifluorescence techniques, where illumination and observation occur from the same side of the sample, do not suffer such limitations allowing the measurements to be performed at optically opaque electrodes. [31-33] Many highly fluorescent dyes are commercially available and have found extensive use in the life science for imaging. One example are the phenoxazinone based dyes which include resorufin, used in cell vitality tests and Nile Red[34] a commonly used lipid soluble dye for cell membrane imaging.

This article presents a combined electrochemical and fluorescence imaging study of an ionic liquid/toluene in water based emulsion dyed with Nile Red. First, the use of fluorescence imaging and particle tracking[35] enables the stochastic sizing of the emulsion. Second, the ability to image the particle adjacent to and at a carbon fibre electrochemical interface is evidenced and the irreversible adsorption of the droplets to the surface exemplified. Third, the electroactivity of the emulsion is evidenced, and it is shown how the fluorescence intensity is sensitive to the electrochemically controlled redox state of the dye dissolved in the droplet. Finally, the work turns to demonstrate how the measurement of the fluorescence intensity of the individual surface bound droplets as a function of the electrode potential allows the effective voltammetric response of an *individual* particle to be constructed from the optical data. This technique allows the dynamic electrochemical response of an ultra-small confined volume (ca. tens of attolitres) to be experimentally recorded, yielding chemical information that is complementary and additional to that obtained from the ensemble electrochemical response.

EXPERIMENTAL SECTION

Chemicals. Trihexyl(tetradecyl)phosphonium trifluorotris(penta-fluoroethyl)phosphate, [P6,6,6,14][FAP], was donated from Merck. Nile Red (99%) (9-diethylamino-5-benzo[α]phenoxazinone) was purchased from Acros Organics part of Fisher Scientific UK Ltd (Loughborough, UK) and both and were used as received without further purification. All other chemicals used were of analytical grade and were purchased from Sigma-Aldrich. Aqueous solutions were made using ultrapure water (Millipore, resistivity not less than 18.2 MΩ cm at 25^{o}C).

Emulsion Synthesis. The ionic liquid/toluene-in-water emulsion has been described previously.[8,36] However, notably in this work the ionic liquid [P6,6,6,14][FAP] has been used in place of its bistriflimide analogue and was mixed with the toluene in a volume ratio of 2:3. The fluorescent dye Nile Red (12 mM) was dissolved in the ionic liquid/toluene mixture prior to its addition to the water. Upon addition of the Nile Red containing organic solvent mixture to the water (1:50 volume ratio), the solution was vortexed for approximately one minute and then sonicated as previously described. This procedure resulted in the formation of a stable suspension (observable agglomeration/precipitation only after 5 days).

Optical Setup and Analysis. Optical measurements were made on a Zeiss Axio Examiner.A1 Epifluorescence microscope using a 20x air objective (NA = 0.5, EC Plan-Neofluar) or 40x oil-immersion objective (NA = 0.7-1.3, plan-Apochromat) and Zeiss filter set 15 (excitation band pass 546±12 nm, emission low pass 590 nm) (Carl Zeiss Ltd., Cambridge UK). Image acquisition was provided by a Hamamatsu ORCA-Flash 4.0 Digital CMOS camera (Hamamatsu, Japan), providing 16-bit images with 4 megapixel resolution. Images were acquired with an exposure time of 10ms. Throughout the work microscope images were acquired at a rate of 10 frames/s. Synchronisation and triggering of the camera was provided externally, see the 'electrochemical equipment' section for more information. Camera exposure control and most image analysis was provided by the software Zen 2 (blue edition, Carl Zeiss Ltd., Cambridge UK). Construction of the fluorescence measured voltammetric responses required calculation of the 1st time derivative of the particle fluorescence intensity. The mean intensity is measured and averaged over the entire image of the particle and normalized against its initial value at the start of the voltammetric scan. Smoothing of the 1st time derivative was achieved using a 2nd order Savitzky-Golay filter, points window size equals fps(Hz) x 100 / scan rate(mV s^{-1}). Further information on the procedure is provided in the SI section 7.

Fluorescent particle tracking was enabled via the use of the Python package Trackpy 0.3.2.[37] This package provides an implementation of the Crocker, Grier[38] algorithm. Removal of static features in the optical images was achieved through a background subtraction, where the time-average microscope image was calculated and subsequently subtracted from each individual frame. Independent validation of the software and microscope setup was enabled via the dark-field tracking and sizing of 50 nm silver nanoparticles, see SI section 1 for further information.

Cell Design. The design for the combined electrochemical/optical cell was adapted from that previously used for 3D nanoparticle tracking,[16] the schematic of which can be seen in the Scheme 1. The cell consists of two carbon fibre electrodes in a cavity between a glass slide and coverslip with the volume sealed using parafilm. The thickness of the cell is in the range of 200-300μm. The cavity is filled via two capillary pipette tips with diameters less than 300 μm (GELoader, Eppendorf, Stevenage UK).

Electrochemical Equipment. Macro-electrode experiments were performed on a glassy carbon (GC) electrode (radius = 1.5 mm, CH Instruments, TX, USA) using a computer controlled μ3Autolab potentiostat (Metrohm Autolab B.V., Utrecht, The Netherlands). A saturated calomel electrode (SCE, BAS inc, Japan) or silver wire (Goodfellow, Cambridge, UK) was used as the reference or pseudo-reference electrode respectively. The cell was completed using a platinum mesh (Goodfellow, Cambridge, UK) as the counter electrode.

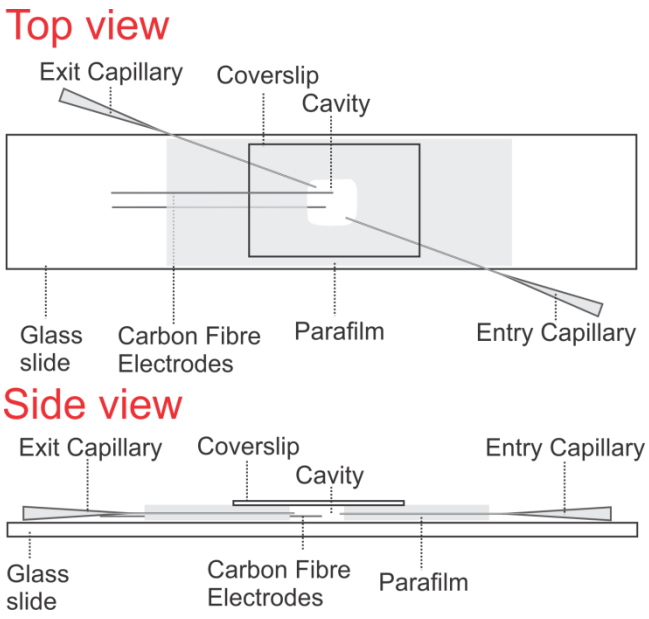

Scheme 1: Cell design used for the combined opto-electrochemical measurements.

Combined opto-electrical measurements were performed using a two electrode setup (cell design described above), where a 7.5 µm diameter carbon fibre wire electrode (Goodfellow, Cambridge, UK) was used as the working electrode. The combined counter/reference electrode comprised of a carbon fibre electrode coated in a thin layer of silver epoxy (RS Components Ltd, UK). Potentiostatic control was provided by an in-house built device, as developed previously for nanoimpact experiments.[39] Control of the working electrode was provided by a highly stabilised (1 kHz bandwidth) classic adder potentiostat, where the working electrode potential is nominally controlled in increments of 60 µV. The analog-to-digital and digital-to-analog conversion was provided by two USB-6003 DAQs (National Instruments, TX, USA).. Control of these devices were performed by a script written in Python 2.7 with a graphical user interface and real-time electrochemical data visualization based upon the packages provided in the Enthought Tool Suite (Enthought, TX, USA). This script also provides the external timing/trigger signal (via a USB-6003) to the microscope camera, hence providing synchronization between the optical and electrical, measurement and control systems (oscilloscope measured delay of less than 1.1 ms between the timing of the potentiostat connection and the initial optical image acquisition, subsequent camera image triggering is hardware timed by the USB-6003). Measurement of the current at the working electrode was achieved using a low current-amplifier DDPCA-300 (Femto Messtechnik GmbH, Berlin, Germany). At a gain setting of 10^8 V/A the bandwidth of the output amplified signal is 150 Hz. The resulting analog signal was oversampled at a stream rate of 5 kHz.

RESULTS AND DISCUSSION

This work starts by characterizing the size of the fluorescent emulsion droplets in solution via single particle tracking analysis. In the thin-layer optical cell it is demonstrated how the droplets can be visualized adjacent to and at an opaque carbon fibre microelectrode, evidencing the accumulation of the droplets at the electrochemical interface. The work then shifts to considering the electrochemical response of these emulsion droplets. First, the ensemble voltammetric response of the Nile Red stained emulsion droplets are studied at a macro electrode. Second, in the combined opto-electrochemical cell the reduction and oxidation of individual surface bound particles in response to the applied electrode potential is monitored optically. Third, cyclic voltammetric experiments are performed on the surface bound particles demonstrating how effective cyclic voltammograms of the individual particles can be reconstructed from the fluorescence microscopy images. The article finishes by discussing and highlighting aspects of the redox chemistry of Nile Red in these confined volumes revealed by the single particle voltammetry technique.

Fluorescent Single Particle Tracking Analysis. Nile Red is a highly fluorescent solvatochromic dye.[34] As the polarity of the solvent increases, the absorption and emission spectra exhibit a bathochromic shift to longer wavelengths. Moreover, the fluorescence quantum efficiency of the species decreases in hydrogen bond donating solvents.[40] The solvatochromic sensitivity of the dye predominantly arises due to the relatively large dipole moments associated with the ground (8.2±1.0 D) and excited (10.0±1.0 D) electronic states of the molecule.[41] Experimentally, in toluene the absorption maxima (λ_{max}) for Nile Red occurs at 524 nm, with the emission spectra maxima shifted by 63 nm to 587 nm. In water the absorption shifts to 584 nm and the fluorescence is found to be significantly weaker but centred at 666 nm.[42] In terms of their solvatochromic shifting of adsorption maxima, ionic liquids tend to behave as moderately polar solvent environments.[43]

The ionic liquid/toluene emulsion was synthesized as described in the experimental section and containing 12 mM of the dye in the emulsion droplets (assuming the dye is solely partitioned to the organic phase). The UV-vis spectrum of the resulting emulsion was recorded, as anticipated the adsorption spectra exhibits a significant amount of scattering due to the presence of the droplets, as evidenced by the high background; however, a clear peak attributed to the absorption of the Nile Red is observed at 548 nm (data shown in SI section 2). This shift in the absorption maxima is consistent with the more polar environment present in the mixed ionic liquid/toluene organic phase as compared to pure toluene.

Fluorescence imaging of the emulsion was achieved through the use of an epifluorescence microscope. The as synthesized emulsion was diluted 100-fold with 50 mM HCl. This acidified suspension was filled into a thin layer optical cell and its contents imaged. Clear visualisation of the emulsion droplets was possible, where in the field of view a large number of bright fluorescent points are observable. A series of images of the emulsion droplets were captured at a rate of 10 frames per second over a 17 second time period. The resulting image stack was analysed, providing an estimation of the trajectory of each individual droplet within the field of view. Due to the relative thickness of the cell it was possible to image the droplets significantly away from the cell walls and hence minimise any possible influence arising from near wall hindered diffusion of the particle at the interface.[44]

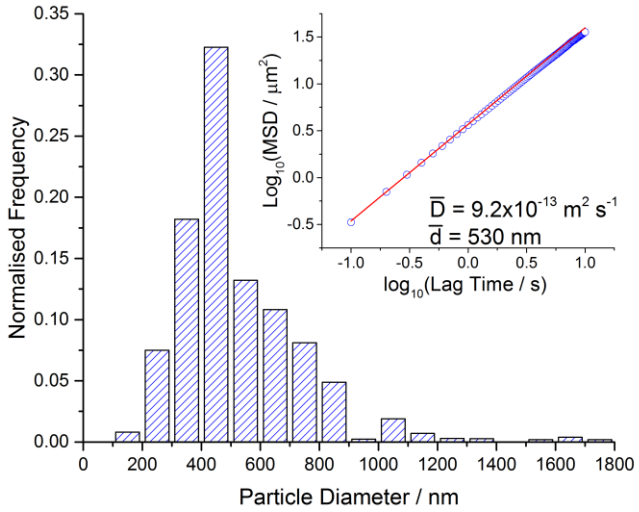

Figure 1: Estimated particle size distribution of the Nile Red stained ionic liquid/toluene-in-water emulsion droplets, as measured from the single particle trajectories. Inlay depicts the ensemble mean-squared-displacement plot from which the ensemble average particle size is determined to be 530 nm (red line: MSD plot fitting using the 2nd-5th lag time points [45]), the particle size interquartile range is determined to be 180 nm.

SI section 3 presents a representative image of the particles in solution and the resulting trajectories analysed over the period of the acquisition. These images are two dimensional (x,y) representations of the particle positions, movement of the particle perpendicular to the field of view (z), leads to the particles moving in and out of focus. Consequently, over the course of the series of acquired images particles may appear and disappear from the field of view. Analysis of the 2D trajectory enables the diffusion coefficient of each particle to be estimated. The mean-squared-displacement (MSD, m^2) as a function of time (t, s) of a particle in two dimensions is related to its diffusion coefficient (D, $m^2\ s^{-1}$) via the following equality:[35]

$$MSD = 4Dt$$

In this work particle trajectories containing less than 30 positions are discarded due to the relatively low accuracy of the associated measured diffusion coefficient. From these individual measurements of the particle diffusion coefficients the particle sizes may be determined through the use of the Stokes-Einstein equation:

$$D = \frac{k_B T}{3\pi\eta d}$$

where k_B is the Boltzmann constant ($1.38\times10^{-23}\ m^2\ kg\ s^{-1}\ K^{-1}$), T is the temperature (K), η is the viscosity of water (8.9×10^{-4} pa s, at 25°C) and d is the particle diameter (m). Figure 1 presents the estimated particle size distribution as measured from a total of 243 individual particle trajectories. The data has been weighted to account for the differing particle trajectory lengths see (SI Section 1 for further details on the analysis procedure). Notably the particle size distribution exhibits a positive skew, with the modal droplet diameter being between 400 and 500 nm. The droplets average diameter is estimated to be 530 nm (interquartile range = 180 nm). Hence the volume of the average droplet is approximately 80 attolitres. Having tracked and estimated the size of the droplets in the solution phase the work now turns to consider the interaction of the Nile Red dye stained emulsion with the carbon fibre electrode in the absence of an applied potential.

Droplet Accumulation at a Carbon Fibre. Beyond visualisation of the droplets in solution the thin-layer optical cell allows observation of the Nile Red stained emulsion adjacent to and at a carbon fibre interface. The ability to image particles at a solid and opaque interface is one of the significant advantages of the use of epifluorescence techniques. Importantly, dark-field imaging, either in two or three dimensions (holographic) suffer from lower signal noise ratios associated with light scattering from the adjacent substrate. This can be even more problematic in the case of the use of thin-layer gold films where the morphology and hence scattering intensities at local surface defects may alter when a potential difference is applied to the interface.[17]

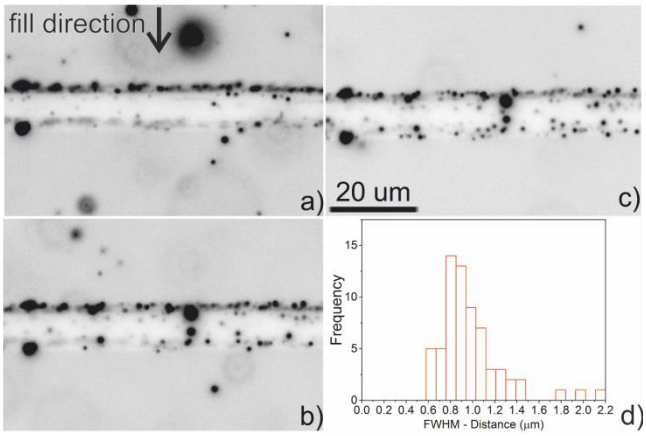

Figure 2: Fluorescence microscope images of a carbon fibre wire submerged in the Nile Red stained ionic liquid/toluene emulsion (1:100 dilution, 50 mM HCl) as a function of time a) 0, b) 10 and c) 30 minutes, all scales are the same as in c). Note the contrast of the microscope images have been inverted for clarity. d) depicts the full-width-half-maximum of the intensity profiles of 66 surface bound droplets measured over a 90 μm length of carbon fibre.

Figure 2 a), b) and c) depict a series of three zoomed images of a carbon fibre submerged in the emulsion (dilution 1:100, 50 mM HCl) at times of zero (a), ten (b) and 30 (c) minutes after the filling of the optical cell. The grey scale image has been inverted for clarity such that the bright emulsion droplets appear as dark points in the image. In Figure 2 a) the carbon fibre wire is clearly visible with a number of emulsion droplets already affixed to its surface. Note the wire is only observable as a silhouette against the relatively bright fluorescence background, consequently fluorescence imaging of the wire prior to filling the cell with the fluorescent suspension is not feasible. In Figure 2 a) the initial position of these droplets on the carbon fibre wire predominantly reflects the flow in the thin-layer cell whilst being filled. Once filled the particles move, by virtue of Brownian motion, within the volume and randomly collide with the carbon fibre. Upon collision the particles are seen to adhere to the wire and remain fixed to its surface. This accumulation of the droplets from solution to the wire is clearly apparent in the timed images shown in Figures 2 a), b)

and c). It should however be commented that these long observation times (30 min) on one area of the electrode lead to the droplets becoming – to an extent – photo bleached, hence the observed intensity of some of the particles present in the first image has decreased over the time course of the accumulation. SI section 4 provides an example of a single particle being tracked in solution and then colliding with the wire and becoming fixed. Once attached to the surface none of the particles under observation have been found to leave the interface.

After collision and attachment to the interface, the intensity profiles of the particles on the surface can be measured. For the present optical system (NA = 0.5, emission low pass filter = 590 nm) the diffraction limited full-width-half maximum (FWHM) of the points intensity profile is approximately ~800 nm in water assuming a wavelength of 600 nm. Conversely, for a sphere *significantly* above the resolution limit of the imaging system and assuming that the fluorophores are uniformly distributed within the droplet volume, then the measured FWHM is equal to $3^{0.5}/2$ times the particle diameter. For a particle of diameter 520 nm the expected FWHM of the image is ~865 nm. Figure 2 d) depicts the measured FWHM of the intensity profiles of particles (n = 66) situated on a 90 µm length of a carbon fibre wire submerged in the emulsion. Errors in the measurement of the FWHM arise due to the image pixelation; moreover, due to the curvature of the wire some of the particles will be less in focus. However, the size of a particles intensity profile as measured via its FWHM gives some insight into the droplet dimensions when situated on the wire. For a more in depth discussion of the relationship between the droplet size and the measured intensity profile FWHM see SI section 5. From Figure 2d) it is notable that the majority of the observed surface bound particles are close to the diffraction limit of the imaging system. Although the two measurements (single particle tracking and FWHM of the intensity profile) of the particle size distribution are not directly comparable, the sizes of the particle measured in the image are consistent with those obtained from the tracking analysis. Consequently, it is concluded that upon adsorption of the particles no appreciable coalescence occurs for the surface coverages presently under study. Noting the precise droplet shape at the interface will be sensitive to the wetting properties of the emulsion at the carbon fibre surface. Having demonstrated the accumulation of the droplets at a carbon surface, the work now reports the ensemble electrochemical response of the emulsion at a macroelectrode.

Emulsion Ensemble Electrochemical Response. A macro glassy carbon electrode was submerged in the ionic liquid/toluene emulsion (1:100 dilution, 50 mM HCl) and the cathodic voltammetric response recorded between 0.4 and -0.3 V vs. a pseudo silver reference electrode. The resulting voltammetry recorded in the presence (12 mM) and absence (0 mM) of Nile Red in the emulsion is depicted in Figure 3. A reversible voltammetric feature centred at -0.09 V vs. Ag is observed. The inlay of Figure 3 depicts the voltammetric response as a function of scan rate and the peak current is found to vary linearly with the experimental scan rate. Hence, although significant reduction is still occurring at high over potentials (cf. -0.3V vs Ag) the voltammetric feature is concluded to be predominantly surface bound. Moreover, variation of the concentration of the Nile Red dissolved in the emulsion is found to scale the magnitude of the voltammetric wave (SI section 6). Hence, in light of these observations and the results of the previous section it is concluded that the voltammetric feature likely corresponds to the redox of Nile Red dissolved in the emulsion droplets adhered to the macroelectrode surface.

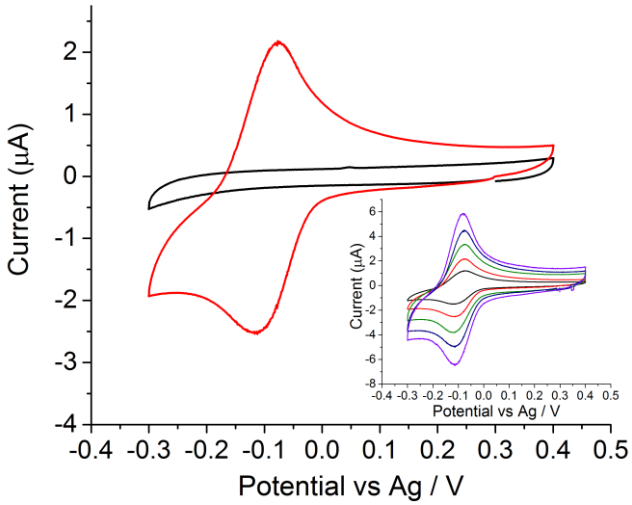

Figure 3: Voltammetric response of the emulsion (1:100 dilution, 50 mM HCl) at a glassy carbon macroelectrode (radius = 1.5 mm) in the presence (red) and absence (black) of 12 mM Nile Red in the emulsion droplets, measured at scan rate of 100 mVs^{-1}. Inlay depicts the same voltammetric wave recorded at scan rates ranging from 0.05-0.4 V s^{-1}.

In order to further illuminate the Nile Red redox process, the voltammetric response of the emulsion at the macro glassy carbon electrode was measured as a function of pH against a saturated calomel electrode (see SI section 6). The position of the voltammetric wave is found to vary with ~60 mV/pH; hence, it is concluded that during the course of the electrochemical reaction an equal number of protons and electrons are transferred. In light of the molecular structure of Nile Red it seems likely that the reversible redox reaction corresponds to the two-electron, two-proton process proposed in Scheme 2. Moreover, the sensitivity of the reaction to the solution phase pH strongly evidences that protons are being transferred into the emulsion droplets so as to protonate the reduced electrochemical species. The article now turns to consider the electrochemical and optical behaviour of the emulsion droplets at a carbon fibre electrode under potentiostatic control.

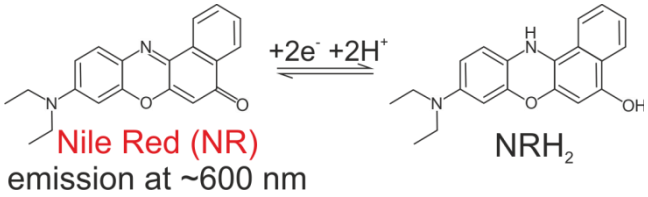

Scheme 2: Proposed redox product and mechanism for the reduction of Nile Red in the ionic liquid/toluene emulsion droplets.

Redox Controlled Fluorescence Switching. In-situ accumulation of the droplets results in a random array of micron and sub-micron sized particles adhered to the electrochemical interface. The developed system allows the synchronisation of

the optical and electrochemical data acquisition systems. Double step chronoamperometry was performed at the carbon fibre wire electrode where the potential was initially stepped to -0.2 V vs Ag for 20 s; following this the electrode was stepped anodically to and held at +0.2 V for a further 20 s. Microscope images were concomitantly acquired at rate of 10 frames per second. Figure 4 depicts the combined electrochemical and optical results. The measured time current profiles (Figure 4 a) predominantly show the current associated with the capacitive charging and discharging of the carbon fibre electrode. Figure 4 b) shows three representative images of the carbon fibre wire during the course of the chronoamperogram. The fluorescence intensity of the surface bound particles is clearly seen to switch off and on as a function of the applied potential.

Analysis of the microscope images allows quantitative information regarding the fluorescence intensity of individual particles as a function of time to be obtained. Overlaid on the electrochemical response of the carbon fibre wire are the measured fluorescence intensities for three arbitrarily selected surface bound Nile Red dye emulsion droplets (Figure 4 a). The values presented are obtained by averaging the digital microscope image intensity over the entire observable area of the each particle for each frame in the time series. The resulting mean intensity versus time plots for the individual particles are subsequently background corrected and normalized against their initial intensity at beginning of the chronoamperometric experiment. As can be seen from the figure, application of the reductive electrode potential (-0.2 V vs. Ag) results in a rapid decrease in the particle fluorescence intensities. The magnitude of these fluorescence intensities decreases to less than twenty percent of their initial values after ca. 10 seconds of the reductive electrode potential being applied. Even after 20 seconds of the reductive potential being applied the particles are still observable in the microscope images albeit with lower fluorescence intensities.

After the reductive chronoamperometric step the electrode potential is increased to a value of +0.2V vs Ag. Upon application of the relatively oxidizing conditions the fluorescence intensity of the droplets is found to increase (Figure 4 a). However, even after 20 seconds of +0.2 V being applied the fluorescence intensity of the particles only returns to less than 80% of its original value. Notably the magnitudes of the fluorescence intensity profiles shown for the oxidative step do not appear to have reached a steady value even after 20 seconds. Hence, it is apparent that the kinetics of the forward and reverse fluorescence switching process – as measured via the individual particle intensities – differ within the microdroplet environment. This question of the kinetics of the redox switching process will be returned to more fully in the following section. First however, this work reflects on the fact that the measured intensity profiles of the particles as a function of the applied potential provide complementary but not identical information to the measured electrochemical flux. Specifically, the fluorescence intensity is sensitive to the local solvent environment and both the redox and *protonation* state of the fluorogenic substance. Hence, additional information is contained in the imaged intensity profile; however, complete interpretation is a more complex task. Second, the ionic liquid/toluene environment is highly viscous where the pure ionic liquid has a reported viscosity of 0.464 Pa s. As an example of this viscosity the diffusion coefficient of ferrocene in pure [P6,6,6,14][FAP] has been reported as $8.6\pm0.2\times10^{-12}$ m^2 s^{-1}.[46] Ion pairing in ionic liquids is known to have a profound effect on the diffusion coefficients of species in such solvents.[47] Given the relatively large dipole moment of the Nile Red, even with the toluene in the emulsion droplets, it is not unreasonable that the diffusion coefficient of the fluorophore in the individual droplets may be very low. Consequently, mass-transport of the Nile Red within the droplet environment may play a significant role in the observed kinetics of the process. For example if the diffusion coefficient of the Nile Red in the droplet is as low as 1×10^{-12} m^2 s^{-1} then the time taken for a molecule to diffuse a distance ($\sim\sqrt{Dt}$) of a micron will be in the order of a second. The article now continues by demonstrating how the electrochemical switching of the fluorescence intensity may be studied dynamically as a function of the applied electrode potential.

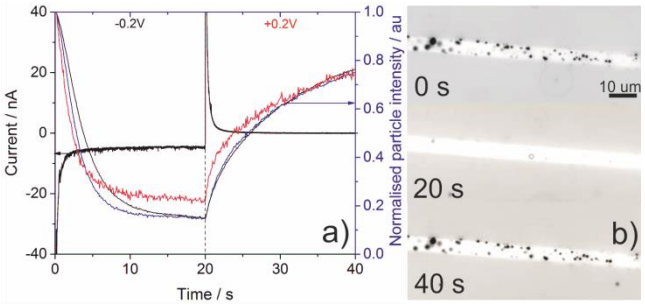

Figure 4: Double step chronoamperometry at a carbon fibre microwire electrode (step 1 -0.2 V vs. Ag for 20 s, step 2 +0.2 V vs. Ag for 20 s). a) depicts the electrochemical current (black) recorded at the entire carbon fibre electrode; overlaid are the fluorescence mean intensity plots (red, blue and grey) for three arbitrarily selected surface bound droplets. The optical intensities have been normalized against their initial values at t=0s. b) shows a series of images of a section of the carbon fibre wire during the course of the chronoamperometric experiment. The fluorescence intensities of the surface adhered droplets can clearly be seen to switch as a function of the applied electrode potential. Note the contrast of the microscope images has been inverted for clarity.

Fluorescence Monitored Single Particle Voltammetry. A number of factors are found to limit the sensitivity of electrochemical measurements of Faradaic currents. Two important factors are the small magnitude of the elementary charge of an electron and the presence of capacitive processes associated with the charging of an electrochemical interface. The vast majority of single entity electrochemical studies achieve detection via the measurement of the chronoamperometric responses. Here a potential is applied to the electrode and during the course of the experiment a single entity be it a cell, nanoparticle or emulsion droplet, may arrive at and collide with the electrode. In this way the electrochemical response of the single entities are temporally decoupled and have improved resolution above the capacitive charging of the electrode. Although this procedure is beneficial in increasing the signal-to-noise ratio, extraction of kinetically useful information commonly requires a series of chronoamperometric measurements to be performed at different potentials. From this series of recorded transients the average response at each potential can be analysed; hence, information about the ensemble kinetics

may be obtained. Although each measurement is itself recorded stochastically on a single entity, information regarding the electrochemical kinetics of and at individual particles is not obtainable. By measuring the fluorescence intensity of individual emulsion droplets the progress of the electrochemical reaction in the small volume (cf. tens of attolitres) can be monitored. Moreover, the differential of mean particle intensity as a function of time yields an indirect measurement of the electrochemical flux. Such measurements are not directly sensitive to the capacitive charging of the electrode and do not suffer issues relating to the measurement of the flux of small charges.

The potential on a carbon fibre electrode submerged in the ionic liquid/toluene emulsion (emulsion dilution 1:100, 50 mM HCl) was initially swept cathodically from 0.4 – -0.3 V vs Ag, the scan direction was subsequently reversed and the potential swept back to +0.4 V vs Ag. During the course of the cyclic voltammetry both the current and the optical response of the surface bound droplets was monitored. Figure 5 depicts the combined optical and electrochemical (inlay) responses of the system at a scan rate of a) 100 mV s^{-1} and b) 10 mV s^{-1}. The optical intensities for three individual particles are presented in Figure 5 as their 1st time derivative. SI section 7 presents the directly measured intensities normalized against their initial intensities. At both 100 and 10 mVs^{-1} a clear quasi-reversible redox wave is observed in the electrochemical response of the wire (Figure 5 a) and b) inlays). The redox process is centred around ~0.0 V vs. the Ag pseudo reference electrode. Notably in the electrochemical response at the lower scan rate (10 mV s^{-1}) a significant number of spikes are observed during the course of the cyclic voltammogram the magnitude of which increase at more cathodic potentials, small numbers of comparable features are also observable in the voltammetric response at 100 mV s^{-1}. These bursts of current are ascribed as relating to the arrival of Nile Red dyed droplets to the working electrode during the course of the electrochemical experiment. The length of the working electrode in the optical cell is approximately ~10 mm. Due to the length of the carbon fibre electrode, the electrochemical noise of the system exhibits a peak-to-peak value of approximately 200 pA. As a consequence of the magnitude of this noise, direct electrochemical single entity detection of the arrival of the droplets to the electrode surface is only feasible for the largest particles present in solution. Second, with the use of a 20x objective the field of view is approximately 665 µm across hence only ca. 15% of the working electrode is observable in the microscope image at any one time, this issue becomes even more apparent with the use of higher magnification. Hence, even though the arrival of a particle may be electrochemically recorded the event itself may occur outside of the optical field of view. This issue is further compounded by the inability to in-situ image the underside of the carbon fibre wire.

Having monitored the fluorescence intensities of three surface bound emulsion droplets during the course of the electrochemical experiment their first time derivatives were calculated and plotted against the applied electrode potential, the results of which are shown in Figure 5. As previously discussed, although the single droplet fluorescence intensities are sensitive to more than just the redox state of the Nile Red dye, at its simplest the time derivatives of the single particle fluorescence intensities can be viewed as single droplet "cyclic voltammograms" measured via the fluorescence intensity. Figure 5 clearly shows the redox switching of the fluorescence as a function of the applied potential and the position of these single droplet fluorescence measured voltammograms are in excellent agreement with that recorded electrochemically for the entire electrode i.e. both processes are found to occur at ~0.0 V vs Ag. Consequently, the differing 'voltammetric' waveshapes observed at 10 and 100 mVs^{-1} can be readily understood as reflecting the change in the diffusion regime within the droplets as a function of the experimental time (scan rate). To explicitly restate this point, at 100 mVs^{-1} insufficient time is given for all of the Nile Red present within the droplets to diffuse through the droplet to the electrochemical interface and undergo reduction, conversely at the lower scan rate of 10 mV s^{-1} nearly all of the redox active material present in the particle is reduced. Hence, the individual particle voltammetric responses at 10 mVs^{-1} exhibit reductive wave-shapes that are highly indicative of thin-layer diffusion within the droplets.

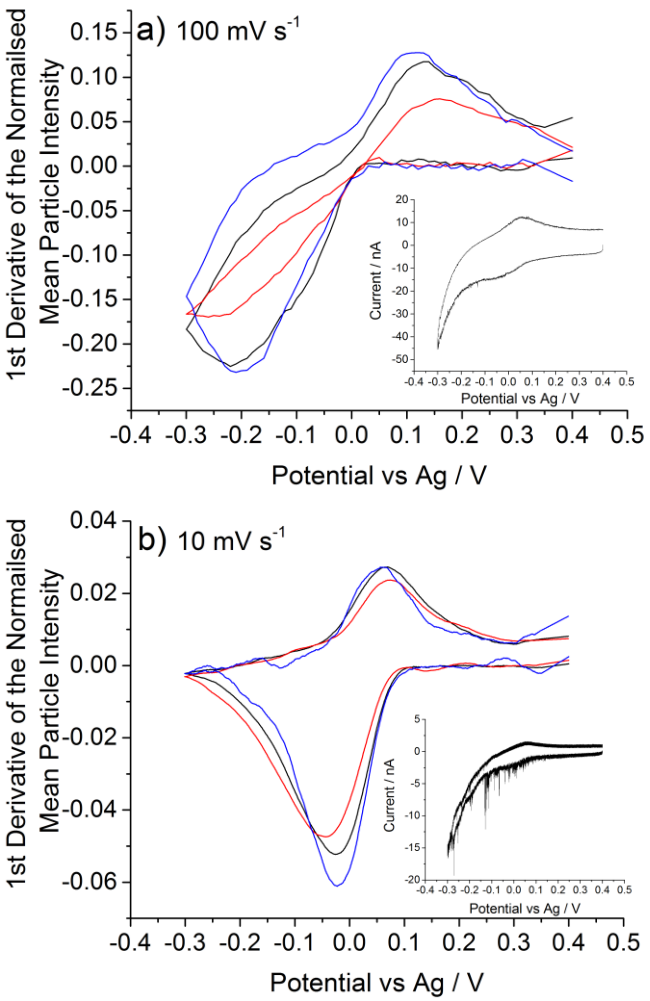

Figure 5: Fluorescence monitored electrochemical flux of three individual droplets from the measurement of the 1st time derivative of the normalised mean particle intensity as a function of the applied electrode potential at a scan rate of a) 100 mV s^{-1} and b) 10 mV s^{-1}. Inlays depict the corresponding electrochemical measurement for the entire carbon fibre electrode.

As discussed previously in relation to the single particle fluorescence responses during the chronoamperometric electrochemical measurements, there is a distinct asymmetry to the kinetics of the reduction and oxidation processes as measured via the droplet fluorescence intensities. For the cyclic voltammetry even at 10 mV s^{-1} the fluorescence intensities of the measured particles at the end of the scan are still increasing however they attain approximately only 70% of their original magnitude. This asymmetry is clearly observable in the reconstructed voltammograms present in Figure 5, where in both cases the magnitude of the anodic peaks are significantly smaller than the associated reductive wave. First, the observed results are *not* consistent with irreversible chemical or photochemical decomposition of the reduced product, as evidenced by the relatively slow increase of the particle intensities towards the end of the cyclic voltammetric scan. This slow increase in the particle intensity indicates that the reformation of the Nile Red is slow and *not* irreversible (see SI section 7 for raw data). Second, this observed asymmetry in the single droplet voltammetry highlights how the presented technique may beneficially provide new and complementary information regarding electrochemical processes occurring in individual confined volumes.

This article finally turns to briefly and non-exhaustively consider the plausible physical origin of this observed asymmetry in the reduction and oxidation processes as measured via the single particle fluorescence intensity. On the basis of the presence of the ionic liquid in the emulsion droplets it is credible that the asymmetry arises due to the differing diffusion coefficients of the oxidised and reduced species in the organic phase. Previous work has demonstrated how for the oxygen/superoxide anion system the diffusion coefficients differ by approximately a factor of 30 due to the relatively strong ion-pairing between the formed superoxide and the ionic liquid cation.[47] SI section 8 presents a simple simulated model of a thin-layer (1 µm) electrochemical cell under a linear diffusion regime where the reduced species has a diffusion coefficient an order of magnitude below than that of the oxidized. Qualitatively this simulated voltammetric response exhibits similar characteristics to those observed in the single droplet voltammetry. However, as demonstrated by the ensemble electrochemical response of the emulsion at the glassy carbon macroelectrode, the position of the redox wave is sensitive to the pH of the aqueous phase. Consequently, it is unlikely that the reduced product is charged and, as such, although its dipole moment will differ from of the parent molecule, it is unlikely that the diffusion coefficient of the reduced and oxidized species differ so dramatically in the absence of ion-pairing with the electrolyte (ionic liquid). As an alternate explanation the sensitivity of the redox response towards the aqueous solution phase pH may give an indication towards the origin of the observed kinetic asymmetry. Specifically, assuming the reduction process corresponds overall to a two-electron, two-proton reduction then seven possible intermediates exist (as may be summarized in a so-called 'scheme of squares')[48,49] and the exact mechanistic pathway taken will be sensitive to the individual pK_as of the intermediates. Moreover, due to the changing electrode potential, for such systems the forward and reverse paths need not be the same.[50] Hence, the reformation of the parent Nile Red molecule may become chemically "gated" by a requirement to deprotonate.

CONCLUSIONS

For the synthesized Nile Red labelled ionic liquid/toluene-in-water emulsion the average droplet diameter is determined to be 530 nm (interquartile range = 180 nm) as measured by single particle tracking analysis. Electrochemically the Nile Red is proposed to undergo a two-electron, two-proton reduction where the product is non or weakly fluorescent. At the single droplet level the kinetics of the reduction and oxidation process is found to be asymmetric, as monitored by the change in the single particle fluorescence intensities. This technique of monitoring the electrochemical flux indirectly via the droplet fluorescence provides a route by which kinetics of an electrochemical reaction can be dynamically probed in an attolitre volume.

ASSOCIATED CONTENT

Supporting Information

This material is available free of charge via the Internet at http://pubs.acs.org. Supporting information provides: validation and further discussion of the details of the single particle tracking procedure (1), the absorption spectra of Nile Red in the emulsion (2), details and representative images of the emulsion tracking (3 and 4), discussion on the resolution of the imaging techniques used (5), ensemble voltammetry of the Nile Red as a function of dye concentration and pH (6), fluorescence intensity profiles during the cyclic voltammetric measurements (7) and a simulation of the electrochemical response of a thin-layer electrochemical cell with significantly different diffusion coefficients or the reduced and oxidised species (8).

AUTHOR INFORMATION

Corresponding Author

* Richard.compton@chem.ox.ac.uk

Author Contributions

‡These authors contributed equally.

ACKNOWLEDGMENT

Mr. B. Briggs and Mr. M. Yang are thanked for recording the UV-vis and fluorescence spectra of the Nile Red in toluene and the emulsion. Mr. P. Hurst is thanked for his help in the production and development of the potentiostat system. The research leading to these results has received funding from the European Research Council under the European Union's Seventh Framework Program (FP/2007-2013)/ERC Grand Agreement No. 320403.

REFERENCES

(1) Gooding, J. J. *Angew. Chem. Int. Ed.* **2016**, *55*, 12956 –12958.
(2) Robbs, P. H.; Rees, N. V. *PCCP* **2016**, *18*, 24812-24819.
(3) Xiao, X.; Bard, A. J. *J. Am. Chem. Soc.* **2007**, *129*, 9610-9612.
(4) Zhou, Y. G.; Rees, N. V.; Compton, R. G. *Angew. Chem. Int. Ed.* **2011**, *50*, 4219-4221.
(5) Fernando, A.; Parajuli, S.; Alpuche-Aviles, M. A. *J. Am. Chem. Soc.* **2013**, *135*, 10894-10897.
(6) Quinn, B. M.; van't Ho, P. G.; Lemay, S. G. *J. Am. Chem. Soc.* **2004**, *126*, 8360-8361.
(7) Cheng, W.; Compton, R. G. *Angew. Chem. Int. Ed.* **2014**, *53*, 13928-13930.

(8) Kim, B.-K.; Boika, A.; Kim, J.; Dick, J. E.; Bard, A. J. *J. Am. Chem. Soc.* **2014**, *136*, 4849-4852.
(9) Sepunaru, L.; Tschulik, K.; Batchelor-McAuley, C.; Gavish, R.; Compton, R. G. *Biomat. Sci.* **2015**, *3*, 816-820.
(10) Sekretaryova, A. N.; Vagin, M. Y.; Turner, A. P. F.; Eriksson, M. *J. Am. Chem. Soc.* **2016**, *138*, 2504-2507.
(11) Tschulik, K.; Compton, R. G. *PCCP* **2014**, *16*, 13909-13913.
(12) Robinson, D. A.; Yoo, J. J.; Castañeda, A. D.; Gu, B.; Dasari, R.; Crooks, R. M.; Stevenson, K. J. *ACS Nano* **2015**, *9*, 7583-7595.
(13) Fosdick, S. E.; Anderson, M. J.; Nettleton, E. G.; Crooks, R. M. *J. Am. Chem. Soc.* **2013**, *135*, 5994-5997.
(14) Hill, C. M.; Bennett, R.; Zhou, C.; Street, S.; Zheng, J.; Pan, S. *J. Phys. Chem. C* **2015**, *119*, 6760-6768.
(15) Nizamov, S.; Kasian, O.; Mirsky, V. M. *Angew. Chem. Int. Ed.* **2016**, *55*, 7247-7251.
(16) Batchelor-McAuley, C.; Martinez-Marrades, A.; Tschulik, K.; Patel, A. N.; Combellas, C.; Kanoufi, F.; Tessier, G.; Compton, R. G. *Chem. Phys. Lett.* **2014**, *597*, 20-25.
(17) Patel, A. N.; Martinez-Marrades, A.; Brasiliense, V.; Koshelev, D.; Besbes, M.; Kuszelewicz, R.; Combellas, C.; Tessier, G.; Kanoufi, F. *Nano Lett.* **2015**, *15*, 6454-6463.
(18) Dick, J. E.; Renault, C.; Kim, B. K.; Bard, A. J. *Angew. Chem. Int. Ed.* **2014**, *53*, 11859-11862.
(19) Caution must be taken in analyzing the measured data so as to suitably account for the possible agglomeration/aggregation state of the material in solution.
(20) Kang, M.; Perry, D.; Kim, Y.-R.; Colburn, A. W.; Lazenby, R. A.; Unwin, P. R. *J. Am. Chem. Soc.* **2015**, *137*, 10902-10905.
(21) Cheng, W.; Batchelor-McAuley, C.; Compton, R. G. *ChemElectroChem* **2014**, *1*, 714-717.
(22) Li, X.; Batchelor-McAuley, C.; Whitby, S. A. I.; Tschulik, K.; Shao, L.; Compton, R. G. *Angew. Chem. Int. Ed.* **2015**, *55*, 4296-4299.
(23) Masa, J.; Batchelor-McAuley, C.; Schuhmann, W.; Compton, R. G. *Nano Res.* **2014**, *7*, 71-78.
(24) Snyder, J.; Fujita, T.; Chen, M. W.; Erlebacher, J. *Nat. Mater.* **2010**, *9*, 904-907.
(25) Banks, C. E.; Davies, T. J.; Evans, R. G.; Hignett, G.; Wain, A. J.; Lawrence, N. S.; Wadhawan, J. D.; Marken, F.; Compton, R. G. *PCCP* **2003**, *5*, 4053-4069.
(26) Marken, F.; Webster, R. D.; Bull, S. D.; Davies, S. G. *J. Electroanal. Chem.* **1997**, *437*, 209-218.
(27) Scholz, F.; Komorsky-Lovrić, Š.; Lovrić, M. *Electrochem. Commun.* **2000**, *2*, 112-118.
(28) Scholz, F.; Schröder, U.; Gulaboski, R. *Electrochemistry of Immobilized Particles and Droplets*; Springer, 2005.
(29) Nakatani, K.; Chikama, K.; Kim, H.-B.; Kitamura, N. *Chem. Phys. Lett.* **1995**, *237*, 133-136.
(30) Nakatani, K.; Sudo, M.; Kitamura, N. *J. Phys. Chem. B* **1998**, *102*, 2908-2913.
(31) Guerrette, J. P.; Percival, S. J.; Zhang, B. *J. Am. Chem. Soc.* **2013**, *135*, 855-861.
(32) Ma, C.; Zaino Iii, L. P.; Bohn, P. W. *Chem. Sci.* **2015**, *6*, 3173-3179.
(33) Doneux, T.; Bouffier, L.; Goudeau, B.; Arbault, S. *Anal. Chem.* **2016**, *88*, 6292–6300.
(34) Greenspan, P.; Fowler, S. D. *J. Lipid Res.* **1985**, *26*, 781-789.
(35) Qian, H.; Sheetz, M. P.; Elson, E. L. *Biophys. J.* **1991**, *60*, 910.
(36) Feng, A.; Cheng, W.; Compton, R. G. *Chem. Sci.* **2016**, *7*, 6458 -6462.
(37) Allan, D.; Caswell, T.; Keim, N.; van der Wel, C., **2016** trackpy: Trackpy v0.3.2 [Data set]. Zenodo DOI:10.5281/zenodo.60550.
(38) Crocker, J. C.; Grier, D. G. *J. Colloid Interface Sci.* **1996**, *179*, 298-310.
(39) Batchelor-McAuley, C.; Ellison, J.; Tschulik, K.; Hurst, P. L.; Boldt, R.; Compton, R. G. *Analyst* **2015**, *140*, 5048-5054.
(40) Cser, A.; Nagy, K.; Biczók, L. *Chem. Phys. Lett.* **2002**, *360*, 473-478.
(41) Kawski, A.; Bojarski, P.; Kukliński, B. *Chem. Phys. Lett.* **2008**, *463*, 410-412.
(42) Fletcher, K. A.; Storey, I. A.; Hendricks, A. E.; Pandey, S.; Pandey, S. *Green Chem.* **2001**, *3*, 210-215.
(43) Byrne, R.; Coleman, S.; Gallagher, S.; Diamond, D. *PCCP* **2010**, *12*, 1895-1904.
(44) Brenner, H. *Chem. Eng. Sci.* **1961**, *16*, 242-251.
(45) Ernst, D.; Köhler, J. *PCCP* **2013**, *15*, 845-849.
(46) Rogers, E. I.; Silvester, D. S.; Poole, D. L.; Aldous, L.; Hardacre, C.; Compton, R. G. *J. Phys. Chem. C* **2008**, *112*, 2729-2735.
(47) Buzzeo, M. C.; Klymenko, O. V.; Wadhawan, J. D.; Hardacre, C.; Seddon, K. R.; Compton, R. G. *J. Phys. Chem. A* **2003**, *107*, 8872-8878.
(48) Jacq, J. *J. Electroanal. Chem.* **1971**, *29*, 149-180.
(49) Batchelor-McAuley, C.; Li, Q.; Dapin, S. M.; Compton, R. G. *J. Phys. Chem. B* **2010**, *114*, 4094-4100.
(50) Savéant, J.-M. *Elements of molecular and biomolecular electrochemistry: an electrochemical approach to electron transfer chemistry*; John Wiley & Sons: Weinheim, 2006; Vol. 13.

TOC